Electric Power Systems Research 186 (2020) 106407

Contents lists available at ScienceDirect

Electric Power Systems Research

journal homepage: www.elsevier.com/locate/epsr

Distributed selective harmonic mitigation and decoupled unbalance compensation by coordinated inverters in three-phase four-wire low-voltage networks

Augusto Matheus dos Santos Alonso[a,b,*], Danilo Iglesias Brandao[c], Elisabetta Tedeschi[b], Fernando Pinhabel Marafão[a]

[a] Group of Automation and Integrated Systems, Sao Paulo State University (UNESP), Av. Três de Março 511, 18087-180 Sorocaba, Sao Paulo, Brazil
[b] Department of Electric Power Engineering, Norwegian University of Science & Technology (NTNU), O.S. Bragstads plass 2, 7491 Trondheim, Norway
[c] Graduate Program in Electrical Engineering, Federal University of Minas Gerais (UFMG), Antônio Carlos 6627, 31270-901 Belo Horizonte, Minas Gerais, Brazil

ARTICLE INFO

Keywords:
Distributed inverters
Harmonic compensation
Power quality
Power sharing
Three-phase four-wire

ABSTRACT

Considering the high penetration of distributed generators in low-voltage grids, establishing a coordinated operation of their grid-tied inverters has become imperative to move towards the implementation of smart grids. Yet, knowing that mitigation of power quality issues such as reactive power, current unbalance and harmonics is of importance within such a context, this work proposes a master/slave control approach, which uses a communication means of low-bandwidth, to flexibly coordinate four-leg inverters dispersed in three-phase four-wire networks. Their coordination is attained by means of a current-based approach, allowing the sharing of active, reactive, harmonic and unbalance currents drawn by loads. The control strategy also regulates the power flow at the point of common coupling of the low-voltage network, while proportionally steering inverters according to their nominal capabilities. In addition to the offering of selective harmonic mitigation, the control approach provides distributed and decoupled unbalance compensation, in partial or total portion, based on concepts from the Conservative Power Theory. Consequently, extraction of sequence components or implementation of virtual impedance control loops are not required. The proposed strategy is evaluated based on multiple simulation results, considering the CIGRE's European low-voltage distribution benchmark, including six distributed inverters, as well as linear and nonlinear loads.

1. Introduction

Dense penetration of distributed generators (DGs) in electrical grids, particularly at the distribution level, is increasing and has been playing a key role in enhancing power system performance by reducing energy losses and supplying additional ancillary services that support the network under critical conditions [1]. In general, DGs providing ancillary capabilities comprise multifunctional control of their power electronic equipment. More specifically, inverters (i.e., DC-AC converters) inserted within a DG infrastructure can flexibly adjust their control references to pursue complementary operational goals beyond their major functionality of active power injection [1,2], such as to provide compensation of undesired currents [3].

In regard to power quality improvement in low-voltage (LV) networks, the exploitation of multifunctional DGs becomes most important in highly-interactive systems such as microgrids (MGs), in which load behavior is dynamic, and the presence of reactive power and circulation of unbalanced and harmonic currents can deteriorate the overall operation of equipment and the grid itself [4,5]. Additionally, the employment of multifunctionalities in distributed generation systems has been primarily discussed in the literature based on the scenario of local applications [6–8]. Thus, since the local control of multifunctionalities, in general, does not consider the concomitant operation of parallel inverters, its adoption may lead to undesired interactions among DGs, as well as potentially causing poor compensation of current and voltage disturbances.

To cope with the challenge of adequately coordinating DGs [9], control strategies have been proposed in the literature, aiming at providing the regulation of active and reactive powers, as well as exploring the provision of ancillary services related to power quality [10–12]. Thus, taking into consideration such a complex matter, relevant works are discussed in the following section, focusing on urgent issues, such as

* Corresponding author.
E-mail address: augusto.alonso@ntnu.no (A.M. dos Santos Alonso).

https://doi.org/10.1016/j.epsr.2020.106407
Received 16 October 2019; Received in revised form 20 March 2020; Accepted 1 May 2020
Available online 22 May 2020

the sharing of reactive, harmonic, and unbalance quantities among DGs in LV networks.

1.1. Literature review

In the literature, methodologies for the coordination of DGs are principally classified into three categories (i.e., centralized, decentralized, and distributed control), depending on how they relate to the use of communication infrastructures [12]. Centralized methods, for instance, rely on data transmission links to exchange information among inverters and a master/central controller. Distributed approaches exchange the control information among the participating agents (i.e., DGs), not depending on a centralized controller, whereas decentralized coordination of inverters generally does not take advantage of communication means. Finally, the concept of hierarchical control [10] has been proposed in the literature using each of the three above-mentioned categories, implementing management systems based on the hierarchy of control layers.

The main benefit of centralized strategies is the provision of accurate control capabilities, precisely regulating active and reactive power sharing, as well as offering harmonic and unbalance mitigation. Nonetheless, the high dependency on communication infrastructures is tied to reliability issues if the system is not well designed. Thus, for instance, if a considerable amount of data needs to be processed over the network, or if faulty and delayed communication channels occur, adequate coordination of DGs may be impaired [13]. The work in [14] is an example of a centralized method, in which DGs under current-controlled mode (CCM) can be steered to share active, reactive and harmonic currents in grid-connected networks based on the concept of virtual admittances. However, mitigation of unbalance currents, and power flow control at the point of common coupling (PCC) of the LV network with the upstream grid, are not addressed in [14]. Another centralized strategy is presented in [15], in which each electrical branch, comprising a DG and local loads, is organized as a nanogrid. Each DG is controlled for the compensation of disturbances caused by the local loads only at their own nanogrid. As a consequence, the scalability of the approach is limited since nodes might exist on which only DGs or loads are connected, and distant DGs are not able to support compensation at other nodes apart from theirs. In [16], a power-based control approach is proposed, based on a master/slave topology, for controlling the power flow with the upstream grid, and for regulating voltage profiles within the network. Nevertheless, the offering of unbalance and harmonic compensation is not discussed. A synergistic strategy is presented in [3] for compensation of undesired currents based on a centralized controller. However, unbalance compensation is not addressed, and the local load currents at the node of each DG are required to be directly measured, which reduces the viability of implementation in networks with highly dispersed loads and inverters.

In relation to decentralized strategies, they are most frequently proposed by taking advantage of droop control [10–12] to steer DGs operating in CCM or voltage-controlled mode (VCM). Nevertheless, the main drawback of droop-based solutions in LV MGs is the limited accuracy on power/current sharing, while coping with acceptable voltage and frequency regulation [17]. The concomitant offering of active, reactive, harmonic and unbalance powers is also another challenge in droop-based strategies [18]. Moreover, most of the droop-based methods still depend on previous knowledge of line impedances or present other limitations related to adequate frequency response [19]. In [20], for instance, fully decentralized control of DGs is attained by modifying P-V droop coefficients, allowing proportional load sharing to be offered among inverters that are driven under VCM [21]. However, being devised for single-phase systems, unbalance compensation is not considered in the method. Another decentralized approach is presented in [22] for compensation of voltage unbalance, along with a damping control that operates in specific P-V droop regions, in which inverters act as resistors in relation to the negative- and zero-sequence components. Harmonics are not tackled in [22] and power flow control at the interconnection with the upstream grid is not addressed. Besides this, extraction of sequence components is, in general, compromised due to noise and harmonic distortions [23]. Decentralized control of DGs for the compensation of unbalance is also proposed in [24] by emulating virtual synchronous generators, using state observers, and model predictive control (MPC). Nonetheless, decomposition of negative sequence components is required and regulation of currents flowing towards the upstream grid does not occur.

Hierarchical control strategies, in contrast, allow us to coordinate inverters by splitting control functionalities in layers that may or may not take advantage of the usage of communication infrastructures [10,11]. For instance, [25] presents a two-layer hierarchical method to steer four-leg VCM DGs based on single-phase droop control and on three independent secondary controllers. Communication is used to feed back voltage signals, striving for the regulation of voltage amplitude and phase, as well as frequency. Although effective performance is attained for unbalance compensation under sinusoidal condition, such work uses virtual impedance loops and needs to extract negative and zero sequence components of voltages, knowing that the effectiveness of both concepts might be affected under non-ideal voltages. In addition, distributed harmonic compensation is not addressed in [25], and the use of the virtual impedance concept may limit the power output capacity of DGs [19].

A distributed and hierarchical strategy, comprising up to a quaternary control level, is discussed in [26], providing accurate active and reactive power sharing based on droop control and a consensus protocol. Although power flow at the PCC is achievable, harmonic and unbalance mitigation is not targeted by the method. Distributed control is also proposed in [27] to accommodate CCM and VCM DGs, taking advantage of communication means to share load currents based on the virtual impedance concept. However, similarly to previous methods, unbalance is treated through the extraction of sequence components. Load sharing based on distributed control is achieved along with voltage quality improvement in an islanded network by a hierarchical approach in [28], in which droop control is integrated to the use of virtual impedances and fundamental sequence component powers.

In [29], a hierarchical power-based approach is proposed to coordinate both single- and three-phase inverters, under CCM and VCM, achieving accurate power sharing, power flow control at the network's PCC, and mitigation of unbalance currents. Nevertheless, a three-phase three-wire topology is studied, and concomitant harmonic compensation is not performed by the DGs. Cooperative sharing of imbalances in four-wire systems based on the Conservative Power Theory (CPT) [30] is proposed in [31], not requiring decomposition of sequence components, consequently enhancing the robustness of the coordinated operation of inverters under distorted voltage conditions, as mentioned. [31] uses a two-layer hierarchical approach for steering DGs under VCM. Its primary layer is ruled by droop controllers, and the secondary layer uses virtual impedance to shape the voltage output of DGs, based on the balanced and unbalanced current parcels defined by the CPT. Although the CPT's unbalanced current definition is adopted, unlike the work proposed here, such a term is controlled as a single component that considers the contribution of both active and reactive unbalance currents [30], not addressing the flexibility to provide decoupled compensation. It is highlighted that, herein, the definition of decoupled currents relies on the orthogonality existing between the active and reactive unbalanced current parcels decomposed by the CPT. This means that such terms are independent from each other and present particular physical interpretations related to, respectively, different conductances and susceptances on the circuit's phases, as comprehensively discussed in [30]. Moreover, in [31], the flexibility to design partial or total compensation of unbalance is not directly addressed, relying on an optimal scheme to limit unbalance compensation and to constrain the output impedance of DGs. In addition, [31] focuses on islanded operation, consequently not addressing power flow control at

Table 1
Summary of Literature Review on Power Quality Improvement Through Parallel Inverters.

Ref.	Control Approach	Topology and Existence of Hierarchy					Power/Current Sharing Functionalities				
		DGs	Central.	Decent.	Dist.	Hierar.	Act.	Reac.	Harm.	Unbal.	PCC Power Flow
3	Supervisory control and local load measurement	1-leg	✓	–	–	No	✓	✓	✓	✗	✗
14	Virtual admittances	3-leg	✓	–	–	No	✓	✓	✓	✗	✗
15	Modified voltage and power control schemes	4-leg	✓	–	–	No	✓	✓	✓	✓	✗
16	Power-based control and local voltage control	1-leg	✓	–	–	Yes	✓	✓	✗	✗	✓
17	Supervisory control, Conservative Power Theory, and local load measurement	3-leg	✓	–	–	Yes	✓	✓	✓	✓	✗
20	Droop control and modified P-V droop coefficient	1-leg	–	✓	–	No	✓	✓	✓	✗	✗
22	Droop control, virtual impedance, and sequence components	1-leg /3-leg	–	✓	–	No	✓	✓	✓	✓*	✗
24	State observers and model predictive control	3-leg	–	✓	–	No	✓	✓	✓	✓*	✗
25	Single-phase droop control Three secondary control systems	4-leg	✓	–	–	Yes	✓	✓	✗	✓*	✗
26	Droop control and four-level distributed controllers	1-leg	–	–	✓	Yes	✓	✓	✗	✗	✓
27	Droop control, and virtual impedance	3-leg	–	–	✓	No	✓	✓	✓	✓*	✗
28	Droop control, virtual impedance, and sequence components	3-leg	–	–	✓	Yes	✓	✓	✓	✓*	✗
29	Power-based control and Steinmetz principle	1-leg /3-leg	✓	–	–	Yes	✓	✓	✗	✓	✓
31	Droop control, Conservative Power Theory, and virtual impedances	4-leg	–	✓	–	Yes	✓	✓	✓§	✓**	✗
32	Current-based control	1-leg	✓	–	–	Yes	✓	✓	✓	✗	✓
33	Supervisory control, Conservative Power Theory, droop control	4-leg	✓	–	–	No	✓	✓	✓	✓**	✗
Here	Generalized current-based control and Conservative Power Theory	4-leg	✓	–	–	Yes	✓	✓	✓	✓	✓

* Extraction of sequence components is required or unbalanced current terms are not decoupled. Flexibility for partial compensation is not addressed.
** Unbalance compensation is addressed based only on the CPT's i_m^u current parcel.
§ CPT's void current parcel is used for the harmonic sharing, along with a virtual impedance shaping scheme.

the PCC under grid-connected mode.

The CPT is also employed in [17], with a four-layer hierarchical architecture and a supervisory controller for load sharing purposes. The strategy uses instantaneous quantities, considers a sequential management of the DGs, and does not offer a current sharing among them that is proportional to their rated power, as done in [32]. Additionally, load currents need to be directly measured, which makes implementation difficult in networks with multiple nodes and dispersed loads. In [33], the CPT and a supervisory control as in [17] are used, in combination with droop control and resistive line impedance compensation. However, power quality improvement at the PCC is achieved based on the local compensation of grouped DGs, and, as in [17], no proportional share among DGs is guaranteed.

A summary of the literature review concerning the use of distributed inverters in LV networks is presented in Table 1. It can be highlighted that the main contribution of this paper lies in proposing an approach to steer dispersed DGs in three-phase four-wire networks, offering a wide range of ancillary services related to power quality, without using sequence components or the concept of virtual impedances. In addition, this study differs from most of other literature works by proposing a method applied to four-leg DGs, such as performed by [21]. Thus, within such a scenario, the strategy provides more flexibility to offer power quality-oriented ancillary services to multifunctional inverters.

1.2. Contributions and paper organization

The main goal of this paper is to propose a coordinated control approach, herein named Generalized Current-Based Control (GCBC), which is formulated under a master/slave hierarchical architecture. The objective of its implementation is to flexibly steer four-leg DGs in three-phase four-wire LV networks, to achieve full controllability of active and reactive currents, as well as to provide distributed harmonic and unbalance compensation seen by the upstream grid. Thus, the main contributions and merits of this work are highlighted as follows:

- The hierarchical GCBC is devised for three-phase four-wire systems, controlling four-leg DGs under CCM, as a further development of the work presented in [32] for single-phase systems;
- Accurate active and reactive current sharing can be offered, concomitantly to distributed and selective harmonic compensation, without requiring the implementation of virtual impedance loops. Moreover, reduction of neutral currents is inherently achieved. The GCBC also allows the possibility to share currents among DGs proportionally, while respecting their nominal current capabilities;
- Another merit of the strategy is the concomitant offering of distributed and decoupled unbalance compensation. The GCBC allows both active and reactive currents to be decomposed onto respective balanced and unbalanced terms. Additionally, the compensation of such unbalance currents can be independently shared among DGs, in partial or full portion. To the best of the authors' knowledge, decoupled compensation of active and reactive unbalance currents has not previously been proposed under a distributed approach considering four-leg inverters. Being devised from the CPT's current decomposition, that feature does not require extraction of sequence components of voltages or currents.

The GCBC holds the same framework as [32], being formulated by only exchanging information about current magnitudes between a centralized controller and each slave unit (i.e., dispersed inverter), which can be fulfilled by a low-bandwidth communication link. No previous knowledge of grid parameters or synchronization among nodes is required, ensuring plug-and-play support of DGs. The control algorithm is implemented focusing on the scenario of LV networks of limited size, such as the CIGRE's European LV distribution benchmark [34] adopted.

This work is organized as follows. In Section 2, the referred LV network is presented, and the hierarchical layers of the control strategy are discussed. The GCBC is devised for three-phase four-wire systems in Section 3, providing the sharing of active, reactive and harmonic currents among DGs. Distributed unbalance compensation based on the CPT is proposed in Section 4. Simulation results are presented in Section 5, and Section 6 provides the conclusions. The CPT's definitions required for this work are presented in Annex A.

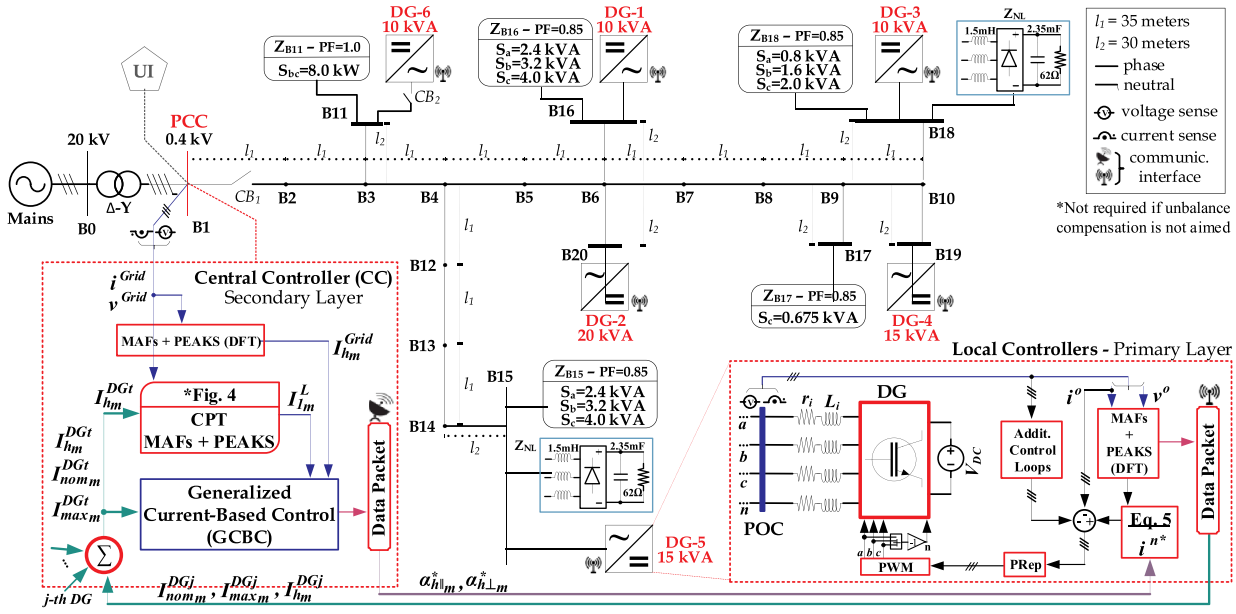

Fig. 1. Considered power system (based on the CIGRE's LV testbench) with dispersed linear and non-linear loads and DGs.

2. Network infrastructure and hierarchical control architecture

2.1. Network topology

The considered system refers to a small size LV network, with a conglomerate of loads and DGs, presenting line impedances with low X/R ratio, being able to also interact with an upstream distribution grid. Although such a topology allows the network to also operate under islanded mode, this scenario of operation is not considered in this work. Under islanded condition, a utility interactive converter (UI) [35] must be placed at the PCC for grid-forming purposes, not affecting the control strategy presented here, as comprehensively described in [32]. A practical example of such topology is the CIGRE's LV distribution benchmark [34], which is herein adopted, as shown in Fig. 1. The infrastructure of the network comprises 20 nodes (B), distributed loads and six DGs with different nominal power capabilities. It considers loads drawing active and reactive power, also featuring unbalance [36]. Yet, to cope with the common challenges of harmonic distortions found in LV grids, the network is adapted by spreading nonlinear loads in some nodes, as shown in Fig. 1. DGs are considered to be driven under CCM. Due to the limited size of the network, it can also be interpreted as a LV MG. It should also be noted that, since the network is a three-phase four-wire system, DGs are implemented with a four-leg topology and are tied to a local point of connection (PoC).

Since the GCBC strategy is formulated under a master/slave framework, it requires a central controller (CC) to act as leading unit. The CC is placed at the network's PCC, providing evaluation of electrical currents flowing through that node. DGs are steered as slave units, changing their local current reference according to control setpoints received from the CC by communication means. In regard to data transmission matters, the adopted network infrastructure also complies with the requirements established on well-recognized standards, such as the IEEE 1547-2018 [37]. Communication among DGs and the CC is realized through narrowband data transmission links of limited performance, using commercialized technologies for inverters, such as the SunSpec Modbus protocol [38]. For instance, baud rates from 9600 to 115,200 bps can be achieved with such technology, which can easily fulfill the requirements of the GCBC algorithm in grids such as the one in Fig. 1. Yet, it also complies with maximum expected latencies of modern communication means applied to electrical systems [27], which are about 100 ms.

2.2. Hierarchical organization

Regarding the control perspective, a hierarchical architecture allows operational functionalities to be organized by layers that consider levels of priority, as well as requirements concerning computational complexity and time processing, as shown in Fig. 2. The required control data is processed under a multi-rate approach that prioritizes, respectively: *i*) reliable nodal operation of inverters; *ii*) coordinated control of distributed DGs; and *iii*) global management of the network and its interaction with the upstream grid. Thus, in accordance with this, lower layers are autonomous on neglecting control setpoints from upper layers if they have the potential to impair robust nodal operation. Although communication is not required for the reliable operation of the primary layer, it may be used to adjust the nodal goals of DGs [32], as done in this work.

In classic hierarchical strategies [10], the secondary layer operates correcting voltage amplitude and frequency deviations, as well as improving the overall performance of poor droop-based coordination. In this work, it is responsible for the coordinated operation of the DGs, as well as for managing the overall network operation. On the proposed master/slave hierarchy, the CC gathers status information from

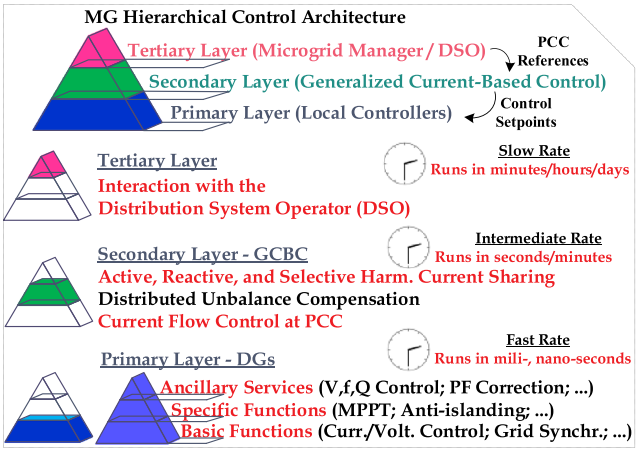

Fig. 2. Hierarchical control architecture with multi-rate operation.

targeted nodes and from every participating DG, monitoring power quality conditions and assessing power flow. Therefore, the GCBC algorithm runs at this layer, as a means for steering DGs to accurately share currents circulating within the network. It allows DGs to supply loads and relieves the LV system from drawing currents from the upstream grid. Since this layer is communication dependent, it runs at a slower rate of milliseconds/minutes to cope with the limitation of low-bandwidth transmission links.

Finally, the tertiary layer incorporates the interaction of the CC with the distribution system operator (DSO) or network manager. This occurs to cope with the possible concept of having a central regulator that assesses the overall operation of clusters of MGs [13], aiming at steering them to achieve power dispatchability at their PCC, consequently adding flexibility to the overall performance of the distribution power system. Therefore, the CC can also be interpreted as an aggregator [39]. By supervising power dispatch, the tertiary layer is processed with rates of minutes to hours, updating the power/current references at the PCC for the GCBC at the secondary layer.

3. Generalized current-based control for three-phase active, reactive and harmonic current sharing

The GCBC strategy is herein presented as an algorithm embedded at the secondary layer of the hierarchical control architecture. The generalization of the previous work in [32], namely CBC, relates to the added possibilities of:

- Sharing active and reactive currents, along with selective distributed harmonic compensation, not only in single-phase circuits, but also in three-phase four-wire systems. Although the GCBC is also suitable for three-phase three-wire circuits, this is outside the scope of this work. Moreover, three-phase four-wire systems comprise a more challenging scenario than three-wire circuits due to the existence of zero-sequence components;
- Considering compensation of unbalanced currents under a distributed approach, decoupling them in active and reactive parcels, and handling them in partial or full portions;
- Achieving three-phase power flow control to the upstream grid.

Such algorithm coordinates dispersed DGs based on the evaluation of currents flowing within the network, computing only peak values of currents. It is devised under a selective approach by dealing with in-phase and quadrature current terms for a set of selected harmonic orders, namely h. The formulation of the GCBC is divided into four main stages, which are: *i)* local evaluation of electrical quantities; *ii)* GCBC processing at the CC; *iii)* acquisition and transmission of data packets; and *iv)* local current reference setting.

3.1. Local evaluation of electrical quantities

This stage has to be processed at each node of interest. This means that each j-th DG should compute the following quantities considering its phase currents and voltages; and likewise, the CC takes responsibility of the same task, processing measured electrical quantities seen by the grid side at the PCC. Such a task starts by using the PoC voltage (v_m^o) as input of a phase-locked loop (PLL) to track the synchronization phase angle (θ_{1m}) of the fundamental component. Index m indicates the phase of the three-phase system (i.e., $m = a,b,c$).

From θ_{1m}, synchronization angles ($\theta_{hm}=h.\theta_{1m}$) for multiple harmonics of interest h (i.e., $h = 3, 5, 7, \ldots, H$) can be attained. Therefore, from θ_{hm}, in-phase and quadrature unity signals, named $x_{h||m}$ and $x_{h\perp m}$, can be calculated from cosine and sine functions, respectively. These calculations are summarized in Fig. 3, also showing the scheme proposed for magnitude calculation.

The peak current terms that need to be processed by the GCBC are then attained based on the previous unity signals (i.e., $x_{h||m}$ and $x_{h\perp m}$) through the implementation of a discrete Fourier transform (DFT) algorithm, which is here devised in time-domain using moving average filters (MAFs). Note that, as the interest here lies in determining in-phase and quadrature peak current terms (i.e., $I_{h||m}$ and $I_{h\perp m}$), the respective output currents (i_m^o) are used as inputs for the DFT algorithm. Yet, any other method [40] for implementing peak detection could also be used without impairing the algorithm. Thus, the attained current terms of targeted harmonic orders are finally gathered on a data packet that is transmitted from each DG to the CC.

3.2. GCBC processing at the central controller

The GCBC algorithm considers a per-phase model which evaluates injected and drawn currents at each phase individually. As a consequence, upon the condition of respecting Kirchhoff's laws, individual operational goals may be set to different phases as desired. Thus, considering the existence of J DGs on the network, the GCBC is processed at the CC based on the following formulation.

Once each j-th DG (with $j = 1, 2, \ldots, J$) sends its data packet to the CC, as discussed in Section 3-C, information on current terms flowing from the entire network is available in relation to each m-phase, and a control cycle k is started. Hence, from (1), the CC calculates the per-phase cumulative contribution of DGs in terms of: injected currents ($I_{h_m}^{DGt}$), their installed nominal capabilities ($I_{nom_m}^{DGt}$), and the actual capacity of active current generation ($I_{max_m}^{DGt}$), where t stands for total. Note that the terms in-phase and quadrature are handled in a separate way and allow selectivity at each harmonic order h.

$$I_{h||_m}^{DGt}(k) = \sum_{j=1}^{J} I_{h||_m}^{DGj}(k) \tag{1.a}$$

$$I_{h\perp_m}^{DGt}(k) = \sum_{j=1}^{J} I_{h\perp_m}^{DGj}(k) \tag{1.b}$$

$$I_{max_m}^{DGt}(k) = \sum_{j=1}^{J} I_{max_m}^{DGj}(k) \tag{1.c}$$

$$I_{nom_m}^{DGt}(k) = \sum_{j=1}^{J} I_{nom_m}^{DGj}(k) \tag{1.d}$$

Sequentially, the aforementioned local evaluation is recalled at the CC, determining the per-phase in-phase ($I_{h||_m}^{Grid}$) and quadrature ($I_{h\perp_m}^{Grid}$) grid peak currents. On the basis of these quantities and Kirchhoff's current law, the load current can be calculated by (2). Note that these are valid due to limited size of the network and the low X/R feature of line impedances, which does not cause significant voltage phase shift among nodes of the power system, as explained in [32].

$$I_{h||_m}^{L}(k) = I_{h||_m}^{Grid}(k) + I_{h||_m}^{DGt}(k) \tag{2.a}$$

$$I_{h\perp_m}^{L}(k) = I_{h\perp_m}^{Grid}(k) + I_{h\perp_m}^{DGt}(k) \tag{2.b}$$

The contributions of the DGs to the network in the next control cycle "$k + 1$" (i.e., the references of peak current terms) are determined based on the desired current flow through the PCC, and the load current to be shared. Thus, the in-phase ($I_{h||_m}^{*}$) and quadrature ($I_{h\perp_m}^{*}$) peak current references are given by (3). Note that the remaining upstream currents desired at the m-th phase, $I_{h||_m}^{Grid*}$ and $I_{h\perp_m}^{Grid*}$, are set by the tertiary control level, and the estimated quantities for the next control cycle $k + 1$ are based on the quantities measured during the last control cycle k. Such remaining currents are responsible for controlling the power flow at the PCC node in Fig. 1 (i.e., upstream currents).

$$I_{h||_m}^{*}(k+1) = I_{h||_m}^{L}(k) - I_{h||_m}^{Grid*}(k+1) \tag{3.a}$$

$$I_{h\perp_m}^{*}(k+1) = I_{h\perp_m}^{L}(k) - I_{h\perp_m}^{Grid*}(k+1) \tag{3.b}$$

Another very important observation is made in regard to the

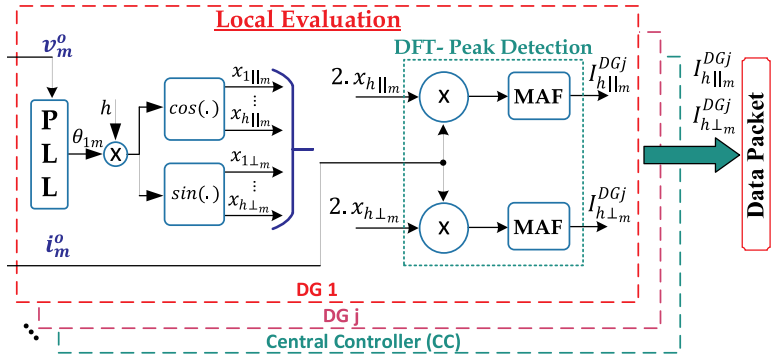

Fig. 3. Local evaluation of electrical quantities.

definitions in (3). At this point, the GCBC allows the provision of active, reactive and harmonic current sharing in three-phase systems, different from [32]. By further exploring (3), unbalance compensation is offered with no further modifications to the GCBC, as explained in Section 4.

Therefore, the coordination of dispersed DGs is determined by the calculation of scaling coefficients that drive the adequate injection of each current term, while considering the current capabilities of the inverters. Such per-phase coefficients, namely $\alpha_{h\|_m}$ and $\alpha_{h\perp_m}$, are sequentially calculated by (4) considering the overall capability of the network ($\sqrt{\Delta I_m}$), later being broadcasted to all DGs participating in the GCBC. DGs' in-phase and quadrature current terms are controlled, respectively, by $\alpha_{h\|_m}$ and $\alpha_{h\perp_m}$. Moreover, the range of these variables is within the interval $[-1, 1; \forall\ \alpha_{h\|_m}$ or $\alpha_{h\perp_m} \in \boldsymbol{R}]$, and can be adapted depending on the features of the considered distributed resource. This means that the GCBC, beyond steering DGs, is able to also accommodate power conditioners, which do not process active power, by only adjusting the use of such coefficients locally (e.g., $\alpha_{1\|_m} = 0$, for active power filters).

$$\alpha_{h\|_m} = \frac{I^*_{h\|_m}(k+1)}{\sqrt{\Delta I_m}}, \quad \forall\ \alpha_{h\|_m} \in \boldsymbol{R};\ -1 \le \alpha^*_{h\|_m} \le 1 \tag{4.a}$$

$$\alpha_{h\perp_m} = \frac{I^*_{h\perp}(k+1)}{\sqrt{\Delta I_m}}, \forall\ \alpha_{h\perp_m} \in \boldsymbol{R};\ -1 \le \alpha_{h\perp_m} \le 1 \tag{4.b}$$

The in-phase component of the fundamental (i.e., $h = 1$), which determines active power flow, is considered first, giving $\alpha_{1\|_m}$. Then, coefficient $\alpha_{1\perp_m}$, which is associated to the reactive current circulation, is computed on the basis of the remaining available current capacity: $\Delta I_m = (I^{DGt}_{nom_m})^2 - (I^{DGt}_{1\|_m})^2$, where $I^{DGt}_{1\|_m}$ is limited to $I^{DGt}_{max\|_m}$. All harmonics with orders higher than the fundamental are considered, sequentially, in the same way, up to the chosen maximum harmonic term H (i.e., $\alpha_{3\|_m}$, $\alpha_{3\perp_m}$, $\alpha_{5\|_m}$, $\alpha_{5\perp_m}$, …, $\alpha_{H\|_m}$, $\alpha_{H\perp_m}$), or up to reaching the nominal current capability of the DG. Since in three-phase four-wire systems triplen harmonics are usually not present or are less significant than others, they can be neglected if desired. Note that the current capacity $\sqrt{\Delta I_m}$ must be recalculated sequentially after determining each in-phase or quadrature scaling coefficient, to avoid overcurrents in steady-state. However, local saturators must be implemented for the inner current control loop within primary controllers to ensure safe transient operation.

3.3. Acquisition and transmission of data packet handling

Since the GCBC methodology is centrally processed in the CC, it depends on communication means to broadcast the control commands (i.e., $\alpha_{h\|_m}$ and $\alpha_{h\perp_m}$) to coordinate the slave DGs. Consequently, specific information must be attained from, and broadcasted to, each DG for the GCBC to operate adequately.

Once a new slave unit is granted participation on the GCBC algorithm, the organization of the data packets being transmitted from this DG to the CC through the communication link should consist of:

- The peak current terms currently being processed by each j-th DG, $I^{DGj}_{h\|_m}$ and $I^{DGj}_{h\perp_m}$. Such information is required for the calculations of (1.a) and (1.b);
- Likewise, the maximum active current, $I^{DGj}_{max_m}$, able to be injected by the local generations should be computed to extract the most active power from DGs;
- Its nominal capacity, $I^{DGj}_{nom_m}$, that must be considered to avoid the assignment of currents exceeding the converter's constraints. Note that, in contrast to the previous quantities, this quantity is determined by the design of the DG, not requiring it to be redundantly transmitted at each data packet gathering window.

The data flow from the CC to DGs requires even less quantities, consisting of the scaling coefficients $\alpha_{h\|_m}$ and $\alpha_{h\perp_m}$ that steer the injection of active, reactive, harmonic and unbalance current terms. Note that, as mentioned, the bidirectional data flow required by the GCBC considers a per-phase analysis of the quantities. Thus, the CC needs to broadcast $2 \cdot h$ coefficients for each phase to be controlled. Nonetheless, as just few quantities are required to be transmitted from/to DGs, low-bandwidth communication links are enough to fulfill such a task [27, 32].

3.4. Local current reference setting

Finally, each DG generates its per-phase current reference (i^{j*}_m) based on its current rating and measured PoC voltage, as given by (5). As done at the CC, the actual per-phase current capability of each j-th DG ($\sqrt{\Delta I^j_m}$) must be recalculated sequentially, after allocating each current term. From (5), it can be proved that the control coefficients $\alpha_{h\|_m}$ and $\alpha_{h\perp_m}$ act scaling the participation of each peak current term processed by the DG.

$$i^{j*}_m = \sum_{h=1,3,5,\cdots}^{H} \underbrace{\left(\alpha_{h\|_m} \cdot \sqrt{\Delta I^j_m}\right)}_{I^j_{h\|_m}} \cdot x^j_{h\|_m} + \underbrace{\left(\alpha_{h\perp_m} \cdot \sqrt{\Delta I^j_m}\right)}_{I^j_{h\perp_m}} \cdot x^j_{h\perp_m} \tag{5}$$

4. Distributed unbalance compensation based on the Conservative Power Theory

The proposed distributed unbalanced compensation is based on the current decomposition provided by CPT [30] (see Annex A), correlating decoupled balanced and unbalanced current terms, with the fundamental peak current terms flowing through the PCC. At this point it is important to recall the concept used in (2.a) and (2.b), which allows the reconstruction of load currents. From the CPT's current decomposition, it can be understood that, within the load active peak current, $I^L_{1\|_m}$, there exists a parcel related to the fundamental balanced current, $I^{L(b)}_{1\|_m}$, plus another term related to the unbalanced one, $I^{L(u)}_{1\|_m}$. Such current

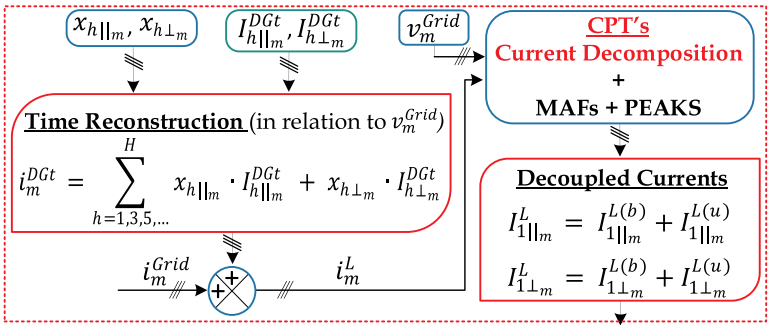

Fig. 4. Proposed scheme for calculation of magnitude of the decoupled unbalance current terms based on the CPT.

terms could also be attained from the peak detection of (A-6) and (A-8) in Annex A (i.e., $I^{L(b)}_{1||_m}$ and $I^{L(u)}_{1||_m}$ relate to the peak of, respectively, i^{b}_{am} and i^{u}_{am}). Similarly, the balanced and unbalanced reactive currents defined by the CPT, given by (A-7) and (A-9), can be related to the fundamental reactive peak current being drawn by the loads, $I^{L}_{1\perp_m}$ (i.e., i^{b}_{rm} and i^{u}_{rm}). As a consequence of identifying such balanced and unbalanced components, they can be selectively handled within the analysis of peak terms shown in Section 3.

Now, refer to Fig. 4 for the following explanations. Since the CPT is time-domain defined, to perform its current decomposition, the instantaneous load currents being drawn within the network must be estimated. Such estimation is done by the GCBC based on the quantities measured on the previous control cycle. At the CC, by computing the peak currents being injected by all DGs, as well as using $x_{h||m}$ and $x_{h\perp m}$, the total current injected by the DGs can be reconstructed in time domain, for each m-phase. Analogous to (2.a) and (2.b), the m-phase instantaneous load current (i^{L}_{m}) can be estimated considering the currents at PCC and summing them with the DGs'. Sequentially, the current terms (A-6) through (A-9) can be obtained from the CPT calculations. Then, by using the same peak detection scheme as Fig. 3, the magnitude of the balanced and unbalanced currents can be decoupled, both for the active and reactive fundamental parcels at a cycle k:

$$I^{L}_{1||_m}(k) = I^{L(b)}_{1||_m}(k) + I^{L(u)}_{1||_m}(k) \quad (6.a)$$

$$I^{L}_{1\perp_m}(k) = I^{L(b)}_{1\perp_m}(k) + I^{L(u)}_{1\perp_m}(k) \quad (6.b)$$

Possessing the balanced and unbalanced current terms, this concept is easily integrated with the GCBC algorithm by relating to (3.a) and (3.b), on which the current references for the next control cycle ($k + 1$) are now obtained by (7). Note that, for the purpose of unbalanced compensation, only the fundamental order is processed in (6), since harmonics practically do not affect unbalance currents. Additionally, by adding the coefficients γ_{Na} and γ_{Nr}, unbalance can be controlled in partial or total portion. In this case, such coefficients range in the interval [0, 1; $\forall\, \gamma_{Na}$ or $\gamma_{Nr} \in \boldsymbol{R}$], acting as the desired amount to be compensated, respectively, for the active and reactive terms. This is an interesting feature for applications in which the load current demand is near or higher to the DGs' capabilities, requiring the reactive, harmonic and unbalance compensation goals to be scaled to best attend the network's operational needs, as in [41]. Again, note that (7) is different and presents more flexibility than the proposals in [17,31,33].

$$I^{*}_{1||_m}(k+1) = I^{L(b)}_{1||_m}(k) + \gamma_{Na}.\, I^{L(u)}_{1||_m}(k) - I^{Grid*}_{1||_m}(k+1) \quad (7.a)$$

$$I^{*}_{1\perp_m}(k+1) = I^{L(b)}_{1\perp_m}(k) + \gamma_{Nr}.\, I^{L(u)}_{1\perp_m}(k) - I^{Grid*}_{1\perp_m}(k+1) \quad (7.b)$$

Finally, it is reinforced that such adaptations to the GCBC algorithm do not change how the algorithm performs, which means that unbalance compensation is added to the strategy, and all the previously presented features are maintained. This is also seen in Fig. 1 by removing the CPT block at the CC. Yet, it is important to highlight that the proposed scheme (i.e., given in Fig. 4) is only implemented at the CC, which presents sufficient computational capability to not further demand intensive processing at the local electronic processors of DGs. Moreover, this does not impair having more information being transmitted among communicating agents.

5. Simulation results of coordinated control by means of the GCBC algorithm

5.1. Simulated environment and control features

To assess the coordination provided by the GCBC strategy, the three-phase four-wire LV network presented in Fig. 1 is implemented in Matlab/Simulink, considering linear and nonlinear loads, as well as six DGs. The parameters of the loads are presented in Fig. 1, being slightly adapted from [36] to facilitate the understanding of this work. To cope with the expected X/R ratio feature of a LV network, the parameters stated in [42] are considered for line impedances (i.e., X/R = 0.12). Nonetheless, higher ratios up to X/R = 0.84 [34] have been tested for this network topology, presenting similar result performance. DGs are composed of four-leg inverters, considering inductive-resistive output filters. Each of their three legs in phases *a, b*, and *c*, is given a reference current to be controlled, and the neutral leg is switched complying with Kirchhoff's current law (i.e., $i^{ref}_{n} = -(i^{ref}_{a} + i^{ref}_{b} + i^{ref}_{c})$). The inner current loop of each inverter is implemented with a proportional-repetitive (PRep) controller designed as in [43], and the DC links are fed by voltage sources. The parameters adopted for the DGs are shown in Table 2.

Communication between DGs and CC is emulated to occur once a cycle, at each period of the 50 Hz fundamental frequency (i.e., 0.20 ms). It is reinforced that adopting such a transmission rate does not impair stability [32], and that the most significant effect of choosing slower transmission rates is related to slower time responses for the control algorithm to achieve steady state behavior.

The simulation results are split into three case studies as follows:

Table 2
Parameters of the network and DGs.

Feature	Specification
Grid line-to-line voltage and frequency	400 V @ 50Hz
DG_1 Nominal Power	10 kVA
DG_2 Nominal Power	20 kVA
DG_3 Nominal Power	10 kVA
DG_4 Nominal Power	15 kVA
DG_5 Nominal Power	15 kVA
DG_6 Nominal Power	10 kVA
DC Link Voltage (V_{DC})	750 V
L Filters Inductor (L_i)	3.5 mH
L Filters Resistance (r_i)	0.10 Ω
DGs Sampling (f_s) and Switching Freq. (f_{sw})	15 kHz
PRep Controllers Proportional Gain (KP_i)	0.56 pu
PRep Controllers Repetitive Gain (K_f)	0.26 pu

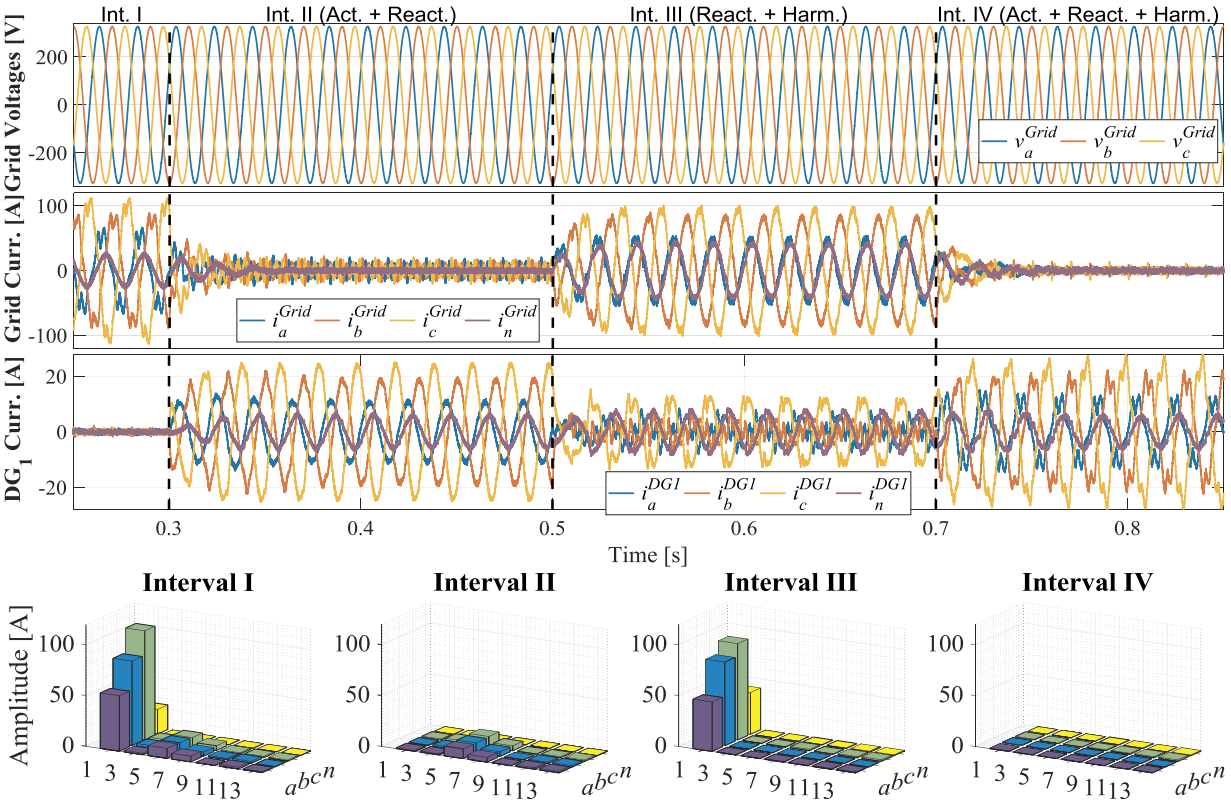

Fig. 5. From top to bottom: Grid voltages and currents, DG_1 currents, and amplitude of grid currents for the most significant harmonic orders, considering phases *a, b, c*, and neutral (*n*), for Case 1. Compensated harmonics are the odd orders from the 3rd up to 13th.

- Case 1: the current sharing capability of the GCBC is evaluated, coordinating DGs to supply the load currents while steering them proportionally to their nominal ratings. This case focuses on demonstrating that the control strategy presented in Section 3 is able to share active and reactive currents in four-wire networks, while concomitantly providing distributed and selective harmonic mitigation;
- Case 2: the proposal within Section 4 is evaluated, demonstrating that this feature can be integrated to the GCBC, allowing the possibility to distributedly share unbalance currents in partial or full portion, while also allowing decoupled active and reactive terms to be compensated as desired;
- Case 3: the ability to provide three-phase power dispatchability at the PCC is presented, and the connection of one extra DG is considered (i.e., demonstrating plug-and-play capability).

For all cases simulated herein, the harmonic set H defined for the GCBC strategy is comprised of the fundamental component plus the odd orders, from the 3rd up to the 13th.

5.2. Simulation results of study cases

5.2.1. Case 1: selective active, reactive and harmonic current sharing

To demonstrate the basic current sharing capabilities of the GCBC algorithm, the result presented in Fig. 5 is taken into account, on which four intervals (Int.) demonstrate the selective and distributed current compensation. Table 3 summarizes the results of this study case, knowing that each interval shows:

- Interval I: DGs are not sharing any current terms;
- Interval II: DGs sharing active and reactive current terms;
- Interval III: DGs sharing reactive and harmonic current terms;
- Interval IV: DGs sharing active, reactive and harmonic current terms.

Table 3
Collective currents [A] at the PCC for Case 1.

GCBC Parcel	CPT Parcel	Interval I	Interval II	Interval III	Interval IV
$I^{Grid}_{1\|\|col}$	$I_{a_{col}}$	95.16	0.18	95.09	0.29
$I^{Grid}_{1\perp col}$	$I_{r_{col}}$	38.77	0.17	1.96	0.22
–	$I_{v_{col}}$	14.75	14.15	2.76	2.44

At first, Interval I in Fig. 5 shows how the grid phase currents are unbalanced, distorted and phase-shifted in relation to phase voltages. The active, reactive and harmonic (i.e., void term, as defined in (A-4) of Annex A) collective currents at the grid side are, respectively, $I^{Grid}_{1\|col} = 95.16\ A$, $I^{Grid}_{1\perp col} = 38.77\ A$, and $I^{Grid}_{v_{col}} = 14.75\ A$. It is reinforced that, since the grid voltage is considered sinusoidal for the following results, the CPT's void current, $I_{v_{col}}$, can be used as an adequate index to quantify the mitigation of harmonics, as the GCBC terms $I^{Grid}_{h\|col}$ and $I^{Grid}_{h\perp col}$ are comprised within $I_{v_{col}}$. Moreover, for the same reason, $I^{Grid}_{1\|col}$ and $I^{Grid}_{1\perp col}$ can be related to the CPT's $I_{a_{col}}$ and $I_{r_{col}}$ current parcels, respectively. From the FFT plots in Fig. 5, it can be noted that the bars of the fundamental components are unbalanced, and total current distortion (THD_i) is 21.42%, 13.59% and 10.40% for phases *a, b*, and *c*, respectively. Neutral current circulates at the grid primarily due to the different current amplitudes drawn at each phase. For this case study, DG_6 remains idle during all intervals.

After 0.3 s (i.e., Interval II), the GCBC starts to steer five DGs (i.e., DG_1 to DG_5) to share active and reactive current terms. In Fig. 5, the currents injected by DG_1 are seen, and in Fig. 6 the collective currents synthesized by all converters demonstrate the proportional sharing provided by the algorithm, according to their capabilities. For instance, note that DG_1 injects half of DG_2's current, as DG_1 presents half of the

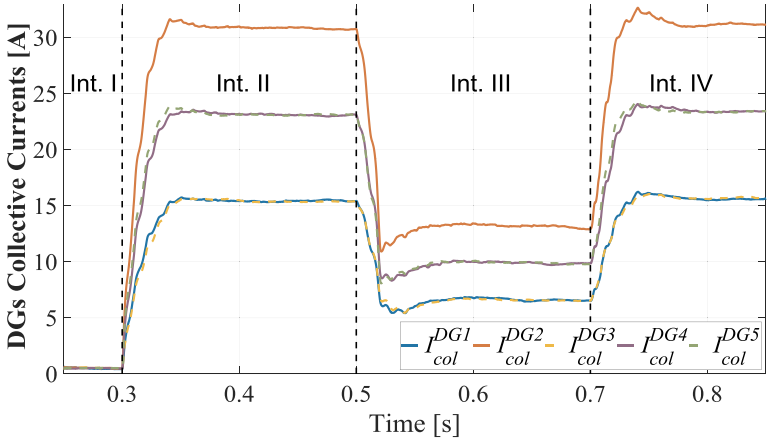

Fig. 6. Collective currents of the three-phase DGs in Case 1.

nominal power of DG_2. Since DGs provide active and reactive current terms for the loads, practically only harmonics flow from the upstream grid, as can be noted by the FFT plot. Then, the amount of collective currents being drawn from the upstream grid is $I^{Grid}_{1\|col} = 0.18\ A$, $I^{Grid}_{1\perp col} = 0.17\ A$, and $I^{Grid}_{v_{col}} = 14.15\ A$. Also note in Fig. 5 that, since the DGs' neutral legs are switched based on the control of the other phases, the inverters operate unbalanced providing null current circulation through the neutral conductor, as seen by the upstream grid.

For Interval III, the GCBC is set to distributedly compensate for reactive and harmonic currents, allowing practically only in-phase unbalanced currents drawn by the loads to flow at the grid side. The final grid currents present THD_i of 6.57%, 3.23%, and 3.78% for phases *a*, *b*, and *c*, and collective values of $I^{Grid}_{1\|col} = 95.09\ A$, $I^{Grid}_{1\perp col} = 1.96\ A$, and $I^{Grid}_{v_{col}} = 2.76\ A$. Since unbalance is not fully compensated, neutral current exists at the grid. Note that, when individually sharing active ($I^{L}_{1\|_m}$) or reactive ($I^{L}_{1\perp_m}$) load currents, the basic definition given in equation (3) is considered, on which balanced and unbalanced current terms are not yet decomposed from each other. Therefore, at this point, it is demonstrated that the GCBC, as presented in Section 3, is not capable of compensating unbalance. This means that the classic GCBC formulation is not able to distinguish the unbalanced currents drawn by loads from their balanced parcels as defined by the CPT. Another important highlight refers to the current $I^{Grid}_{v_{col}}$, which is not fully compensated because the GCBC is only targeting a limited number of harmonic terms (i.e., from 3rd to 13th). This means that most of the remaining distortion currents are composed of higher harmonic orders than the ones tackled.

Finally, in Interval IV the GCBC capability to steer DGs to provide zero power flow at the PCC node is shown, allowing active, reactive and harmonic currents to be shared in three-phase systems. By doing so, as seen in Figs. 5 and 6, DGs inject load currents proportionally to each other, and the network is relieved from drawing power from the upstream grid. Note on the FFT plot that the fundamental and all tackled harmonics are significantly compensated, remaining at the grid, $I^{Grid}_{1\|col} = 0.29\ A$, $I^{Grid}_{1\perp col} = 0.22\ A$, and $I^{Grid}_{v_{col}} = 2.44\ A$.

5.2.2. Case 2: partial and total unbalance compensation

The matter of unbalance compensation is now addressed with the same five DGs sharing different parcels of the load currents during the seven intervals, depicted in Fig. 7 and summarized in Table 4, demonstrating:

- Interval I: DGs are not sharing any currents;
- Interval II: DGs are sharing active currents (balanced + unbalanced), and balanced reactive currents;
- Interval III: DGs are sharing active currents (balanced + unbalanced), and unbalanced reactive currents;
- Interval IV: DGs are sharing balanced active current, and reactive currents (balanced + unbalanced);
- Interval V: DGs are sharing unbalanced active current, and reactive currents (balanced + unbalanced);
- Interval VI: DGs are sharing unbalanced active current, harmonics, and reactive currents (balanced + unbalanced);
- Interval VII: DGs are sharing balanced reactive current, harmonics, and 50% of unbalanced active and reactive currents.

Interval I shows the same initial stage of the previous study case, with the DGs idling, and resulting in $I^{Grid(b)}_{1\|col} = 92.19\ A$, $I^{Grid(u)}_{1\|col} = 23.48\ A$, $I^{Grid(b)}_{1\perp col} = 35.01\ A$, $I^{Grid(u)}_{1\perp col} = 16.60\ A$, and $I^{Grid}_{v_{col}} = 14.75\ A$. The coefficients γ_{Na} and γ_{Nr} are set to one from Intervals II to VI.

From 0.3 s, the GCBC algorithm is enabled considering the CPT's current decomposition scheme of Fig. 4 and Section 4. Harmonic compensation is not set at the first simulated stages to demonstrate the decoupled fundamental sharing of currents by DGs. Nonetheless, it is integrated to the method on the last two intervals to show concomitant operation. As seen in Figs. 7 to 10, DGs proportionally share currents in Interval II, allowing only reactive unbalanced and harmonic currents to flow through the grid. Note that currents are distorted and phase-shifted in relation to the grid voltages (see zoomed view in Fig. 7). Neutral current also exists at the grid due to the circulation of unbalanced reactive parcels at the three phases. From the collective value of currents calculated at the grid, and shown in Fig. 9 and Table 4, it can be re-stated that reactive unbalance is the most significant parcel remaining, with $I^{Grid(u)}_{1\perp col} = 20.52\ A$, while $I^{Grid(b)}_{1\|col} = 2.64\ A$, $I^{Grid(u)}_{1\|col} = 1.18\ A$, $I^{Grid(b)}_{1\perp col} = 3.01\ A$, and $I^{Grid}_{v_{col}} = 14.75\ A$. Although the transient response of the system is a few cycles slow due to the dynamic of the CPT calculation at the CC, it also does not impair stability nor cause deterioration in performance for the strategy. From the FFT plots in Fig. 8, it is seen that only a small amount of unbalance remains for the fundamental term, and harmonic amplitudes remain practically unaltered.

In Interval III, the GCBC changes the control approach to share active (balanced + unbalanced) plus unbalanced reactive currents. By doing so, practically only balanced reactive and harmonic currents flow through the grid, with magnitudes of $I^{Grid(b)}_{1\perp col} = 39.01\ A$ and $I^{Grid}_{v_{col}} = 14.24\ A$. The existence of such reactive parcels can be noted in Fig. 7 (see zoomed view) by the balanced and phase-shifted PCC currents. As a consequence, the GCBC is capable of balancing the conductances and susceptances seen at the PCC, similar to the local strategy presented in [44], but in a distributed way. By imposing balanced currents at the grid, neutral currents are consequently shared among DGs as well.

Interval IV shows full compensation of reactive

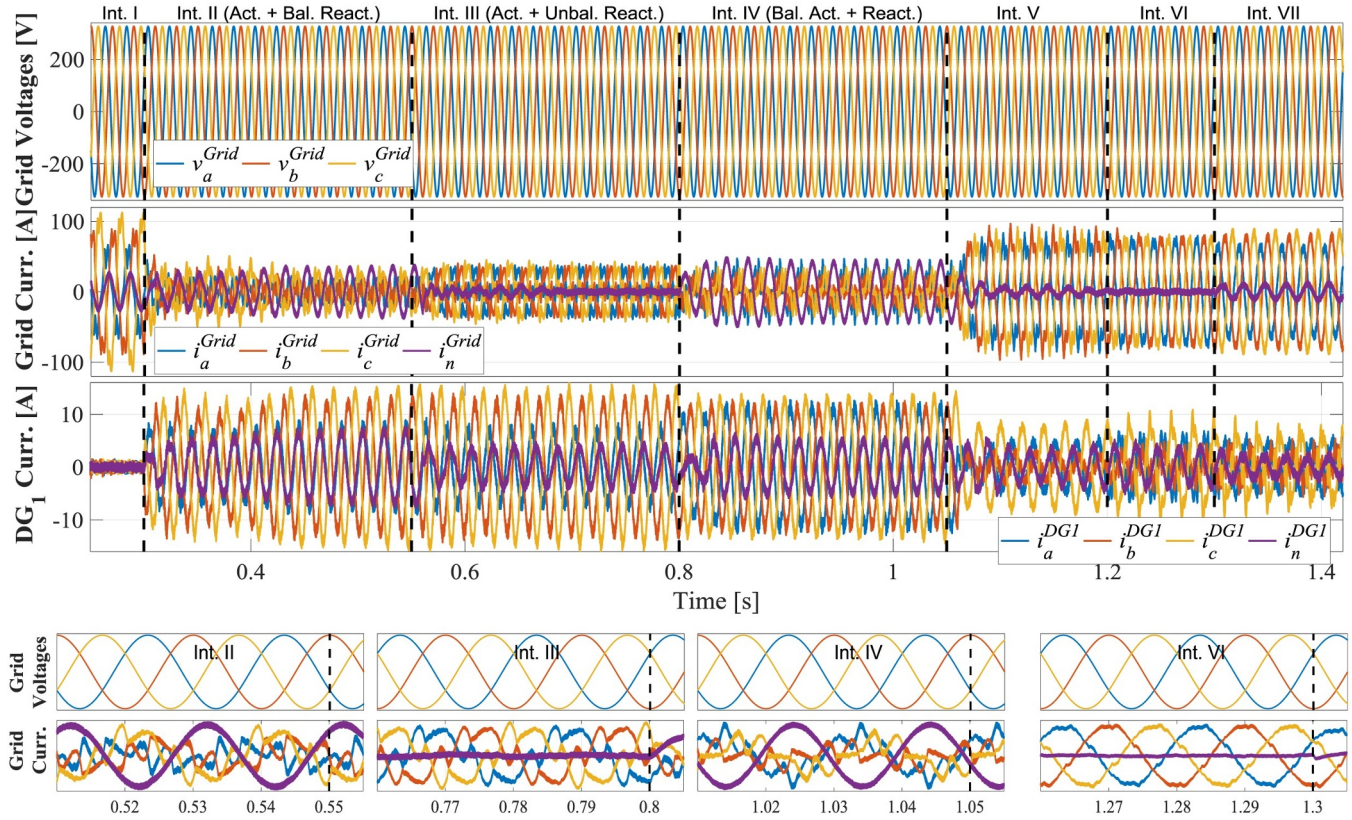

Fig. 7. From top to bottom: Grid voltages and currents, and DG_1 currents for Case 2.

(balanced + unbalanced) terms, along with the injection of balanced active currents. As a consequence, distorted and in-phase unbalanced currents flow through the grid, with collective values of $I_{1||col}^{Grid(u)} = 24.10\ A$ and $I_{v_{col}}^{Grid} = 14.01\ A$. From the FFT in Fig. 8 is seen that, since active unbalance is more significant than the reactive unbalanced currents, the neutral current is higher in Interval IV than in Interval II.

The next interval shows that reactive (balanced + unbalanced) and unbalanced active currents can be mitigated distributedly, while proportionally sharing the burden among DGs, without affecting the active power delivery to loads. Due to the significant compensation of reactive and unbalance terms (see Table 4), grid currents are practically in-phase and balanced, additionally presenting low neutral currents. It is reinforced that, since harmonic sharing is disabled, PCC currents are still distorted. Moreover, THD_i is 15.31%, 14.87%, and 15.74% for phases *a, b*, and *c* respectively. Sequentially, in Interval VI, harmonic compensation is added to the GCBC operation, steering DGs to provide high power factor at the PCC (i.e., PF = 0.998, calculated based on [30]), with much lower current distortion, presenting THD_i of 4.21%, 4.01%, and 4.94% respectively.

Finally, to demonstrate the flexible feature of partially compensating unbalanced current terms, the previous scenario is adjusted in Interval VII by setting γ_{Na} and γ_{Nr} equal to 0.5, aiming at providing compensation of 50% of, respectively, the active and reactive unbalanced current parcels. It is seen in Fig. 7 that grid currents are again unbalanced, but still less than on Interval I. Now, $I_{1||col}^{Grid(u)} = 11.75\ A$ and $I_{1\perp col}^{Grid(u)} = 8.91\ A$, which represent compensation of 50.04% and 53.67% respectively for the active and reactive unbalanced collective currents. The remaining currents present THD_i of 3.65%, 2.45%, and 2.47% respectively for phases *a, b*, and *c*.

5.2.3. Case 3: power flow control at PCC and connection of additional DG

This last case study demonstrates the controllability of three-phase power flow at the PCC, also presenting the GCBC's adequate operation under connection of an extra DG. Thus, three simulated intervals demonstrate:

- Interval I: 5 DGs sharing active, reactive, unbalance and harmonic current terms;

Table 4
Collective currents [A] at the PCC for Case 2.

GCBC Parcel	CPT Parcel	Interval I	Interval II	Interval III	Interval IV	Interval V	Interval VI	Interval VII
$I_{1\|\|col}^{Grid}$	$I_{a_{col}}$	95.16	2.90	0.61	24.11	91.12	91.54	91.71
$I_{1\perp col}^{Grid}$	$I_{r_{col}}$	38.77	20.72	38.97	3.07	1.33	0.93	8.88
$I_{1\|\|col}^{Grid(b)}$	$I_{a_{col}}^{b}$	92.19	2.64	0.09	0.50	91.11	91.53	91.02
$I_{1\perp col}^{Grid(b)}$	$I_{r_{col}}^{b}$	35.01	3.01	39.01	0.30	0.95	0.40	0.10
$I_{1\|\|col}^{Grid(u)}$	$I_{a_{col}}^{u}$	23.48	1.18	0.59	24.10	4.16	1.22	11.75
$I_{1\perp col}^{Grid(u)}$	$I_{r_{col}}^{u}$	16.60	20.52	1.16	0.25	0.95	0.85	8.91
–	$I_{v_{col}}$	14.75	14.36	14.24	14.01	14.38	4.02	2.25

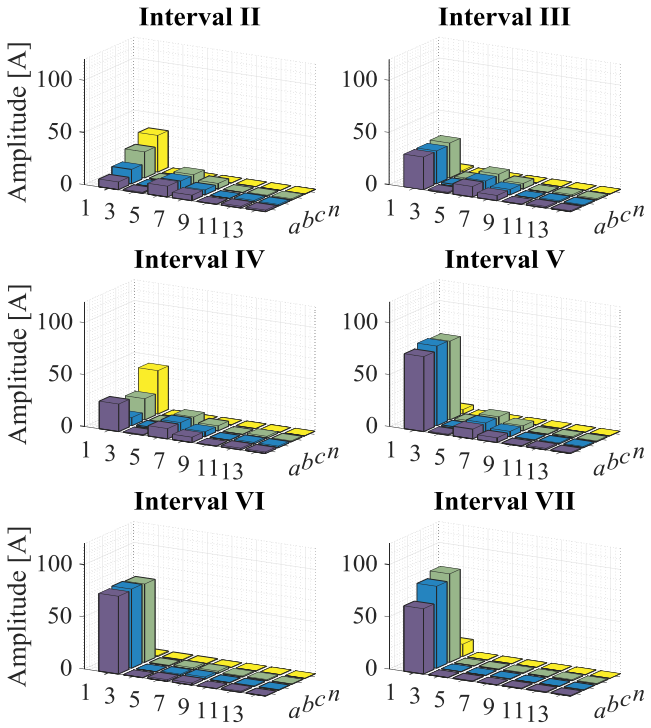

Fig. 8. Amplitude of grid currents for the most significant harmonic orders, considering phases *a, b, c*, and neutral (*n*), for Case 2. Compensated harmonics are the odd orders from the 3rd up to 13th.

- Interval II: One extra DG is connected to support the previous active, reactive, unbalance and harmonic current sharing;
- Interval III: 6 DGs sharing active, reactive, unbalance and harmonic current terms, and the network dispatches active currents to the upstream grid.

The simulation results for the three intervals are shown in Figs. 11 and 12, and the attained current flow through the PCC is summarized in Table 5. For the first interval, the sharing of active, reactive, unbalance, and selected harmonic current terms among DGs is shown to be effective, as the targeted components are practically null. Note that, as expected, this result is the same as in Interval IV presented for study case 1. Then, Interval II begins at 0.85 s, when DG_6 is connected and starts participating in the current sharing provided by the GCBC. As a consequence, the amount of collective current injected by each DG is readjusted by the strategy, as seen in Fig. 12, whereas the proportionality among the currents shared by the DGs is maintained. This transition occurs smoothly and does not cause overcurrents, as shown in Fig. 11. The current measurements at the PCC in Interval II present a similar pattern in relation to Interval I, with practically full compensation of the targeted terms, which proves that the accommodation of more DGs is easily attained with the GCBC.

Finally, after 0.9 s (i.e., Interval III), the previous load sharing of Interval II is adjusted by steering all 6 DGs to, additionally, dispatch active power through the PCC. Thus, by setting a reference of 50 A_{pk} to the PCC current ($I^{Grid*}_{1||_m}$), only balanced active current is dispatched by the inverters. Note in Fig. 11 and Table 5 that practically only in-phase fundamental current flows through the grid. A small amount of high order harmonic currents exist (i.e., I_{vcol} is not null), since they are not targeted by the compensation. Thus, the remaining active power flow through the PCC is $I^{Grid(b)}_{1||_{col}} = 61.47\ A$, which is equivalent to desired per-phase peak current in a balanced system (i.e., $61.47 \cdot (\sqrt{2}/\sqrt{3}) = 50.19\ A_{pk}$). Dispatchability of reactive power could also be straightforwardly implemented with GCBC in a similar fashion, and it shall be considered in future works.

6. Conclusions

In this paper, a hierarchical control approach based on a master/slave architecture was proposed with the goal of steering four-leg DGs in three-phase four-wire LV networks. The so-called GCBC strategy was able to proportionally coordinate several DGs to provide accurate active current sharing, as well as to offer ancillary services related to the distributed compensation of reactive, unbalance and harmonic current terms drawn by the existing loads. Thus, power quality improvement was achieved without requiring the employment of additional power conditioning equipment, such as active power filters. Beyond the fact that distributed harmonic mitigation was attained under a selective manner, compensation of unbalance currents was flexibly provided in a decoupled way by employing the CPT's current decomposition. Thus, as seen by the upstream grid at the PCC, such approach allows the possibility to characterize unbalance currents circulating at the network as uneven conductances and susceptances among the three phases. Such characterization is achieved only by the decomposition of the CPT's active and reactive unbalance currents. Consequently, such unbalance components can be diminished independently, in full or partial portion, in a distributed way through the GCBC approach. Regardless of the operation mode, the GCBC was also able to proportionally steer DGs according to their power capabilities, providing a plug-and-play feature that facilitates its practical implementation. Most importantly, the GCBC does not require any previous knowledge about the network, such as the features of line impedances and network topology.

Simulation results showed that each of the operational assumptions related to the offering of ancillary services can be provided without

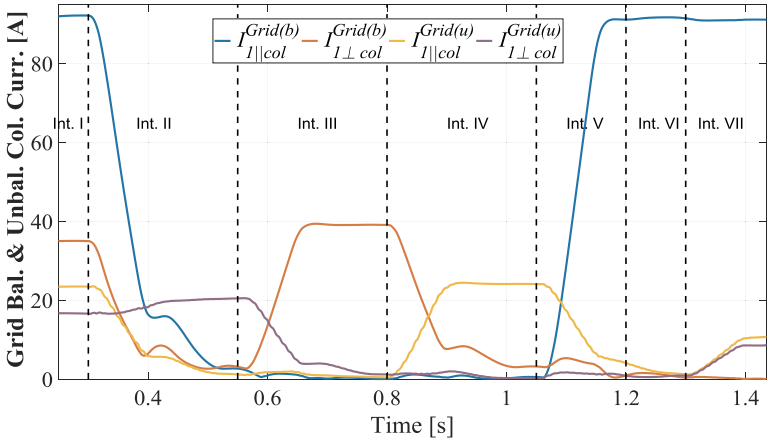

Fig. 9. Grid collective currents in Case 2.

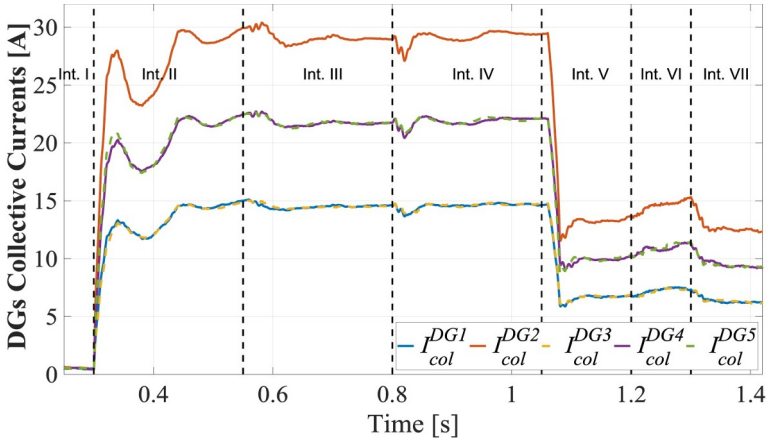

Fig. 10. Collective currents of the three-phase DGs in Case 2.

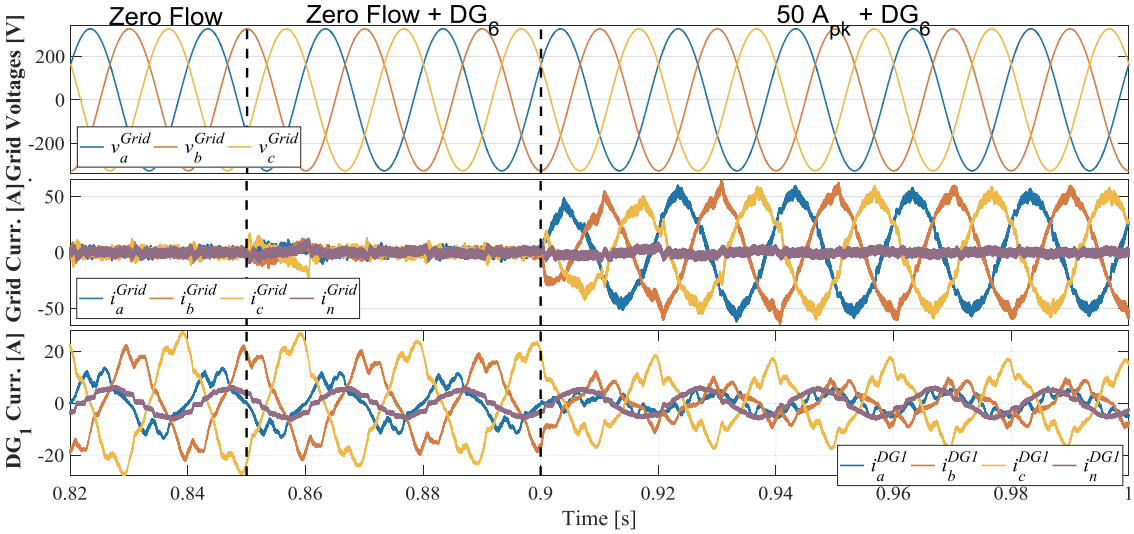

Fig. 11. From top to bottom: Grid voltages and currents, and DG_1 currents for Case 3.

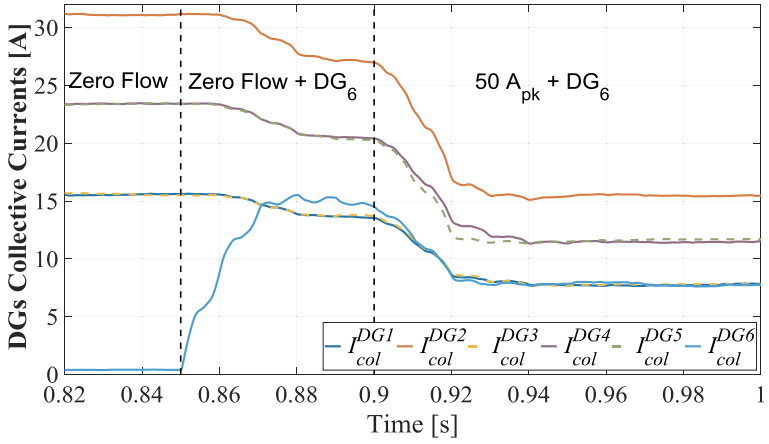

Fig. 12. Collective currents of the three-phase DGs in Case 2.

affecting others, such as demonstrated by the active, reactive, unbalance and harmonic current sharing capabilities of the proposed method. For instance, when the GCBC approach steered DGs for sharing load currents, the LV network was seen by the upstream distribution grid as a single entity which practically did not draw any currents, which facilitates power dispatch and supports stability robustness on the main power system. Additionally, when distributed unbalance compensation was deployed, the proposed strategy allowed the possibility to flexibly balance the PCC currents without implementing concepts such as decomposition of sequence components [46] and virtual impedances. Therefore, knowing that LV networks are prone to operate under distorted voltages, as well as that the implementation and understanding of these two concepts are not trivial, especially under non-sinusoidal voltage conditions, the GCBC strategy seems more

Table 5
Collective currents [A] at the PCC for Case 3.

GCBC Parcel	CPT Parcel	Interval I	Interval II	Interval III
$I_{1\|\|_{col}}^{Grid}$	$I_{a_{col}}$	0.29	0.45	61.47
$I_{1\perp_{col}}^{Grid}$	$I_{r_{col}}$	0.22	0.27	0.96
$I_{1\|\|_{col}}^{Grid(b)}$	$I_{a_{col}}^{b}$	0.01	0.35	61.45
$I_{1\perp_{col}}^{Grid(b)}$	$I_{r_{col}}^{b}$	0.14	0.23	0.94
$I_{1\|\|_{col}}^{Grid(u)}$	$I_{a_{col}}^{u}$	0.29	0.27	0.24
$I_{1\perp_{col}}^{Grid(u)}$	$I_{r_{col}}^{u}$	0.14	0.13	0.10
–	$I_{v_{col}}$	2.44	2.53	2.51

advantageous. Moreover, especially due to the flexibility of steering four-leg DGs for compensating unbalance in four-wire circuits, reduction of neutral currents was inherently achieved by the method.

Since LV networks operating interconnectedly to an upstream grid comprise DGs, it also of importance to control how power is dispatched. Thus, it was shown in this study that the GCBC approach provides three-phase controllability of the power flowing through the network's PCC, coordinating DGs to share the burden of providing load currents, and concomitantly dispatching active power to support the upstream grid. As a consequence of being practically self-sustainable in terms of active, reactive, and harmonic power processing, as well as by allowing only active power to flow at the PCC, the LV network managed by the GCBC can also be interpreted as a dispatchable single entity, as seen by the upstream distribution system. Finally, future works principally intend to: *i)* validate the adequate operation of the proposed strategy upon existence of distorted voltage conditions; *ii)* investigate power quality improvement not only at the PCC, but also on inner nodes of the network; *iii)* provide an experimental validation of the unbalance compensation approach, concomitantly to the three-phase reactive and harmonic mitigation; *iv)* formulate an optimal problem allowing ancillary services to be offered according to the needs of the network manager, as well as upon the consideration of having DGs operating under limited power capability.

CRediT authorship contribution statement

Augusto Matheus dos Santos Alonso: Conceptualization, Methodology, Validation, Formal analysis, Investigation, Writing - original draft. **Danilo Iglesias Brandao:** Conceptualization, Methodology, Writing - review & editing. **Elisabetta Tedeschi:** Conceptualization, Writing - review & editing, Supervision, Project administration. **Fernando Pinhabel Marafão:** Conceptualization, Methodology, Writing - review & editing, Supervision, Project administration.

Declaration of Competing Interest

The authors declare that they have no known competing financial interests or personal relationships that could have appeared to influence the work reported in this paper.

Acknowledgements

The authors are grateful to the Sao Paulo Research Foundation (FAPESP) (Grants 2018/22172-1, 2017/24652-8, 2016/08645-9), and the Research Council of Norway (Grant f261735/H30).

Annex A

The CPT is a time-domain power theory that can be applied to single- or poly-phase systems with periodic quantities, regardless of voltage conditions. Current and power components are decoupled based upon the conservativeness of the active and reactive power terms. The CPT's definition of power terms and corresponding decomposed current parcels is thoroughly discussed in [30] and [45]. The important definitions concerning this work are the ones which follows.

Considering instantaneous and RMS quantities described, respectively, by lowercase and uppercase variables, the active power (P) defined by the CPT in a three-phase circuit is given by (A-1), where v_m is the m-phase voltage, i_m is the line current, and T is the period of these signals.

$$P = \frac{1}{T}\sum_{m=a,b,c}\int_0^T v_m i_m dt = \frac{1}{T}\int_0^T (v_a i_a + v_b i_b + v_c i_c)dt \tag{A-1}$$

Similarly, the reactive power (Q) is defined by (A-2), where $\hat{v}_m$ is the unbiased-time integral of voltage, which is calculated by attaining the integral of v_m and removing its mean value (i.e., $\hat{v}_m = \int_0^t v_m d\tau - \frac{1}{T}\cdot\int_0^T v_m dt$), while ω_0 is the fundamental angular frequency.

$$Q = \frac{\omega_0}{T}\sum_{m=a,b,c}\int_0^T \hat{v}_m i_m dt = \frac{\omega_0}{T}\int_0^T (\hat{v}_a i_a + \hat{v}_b i_b + \hat{v}_c i_c)dt \tag{A-2}$$

In possession of P and Q, the m-phase currents are decomposed into orthogonal terms, comprising both balanced and unbalanced load features, in addition to a remaining component (namely, void), which stands for nonlinearities in currents. Considering the subscripts a, r, and v, respectively, for the active, reactive and void terms, and the superscripts b and u for the balanced and unbalanced features of such parcels, the CPT's instantaneous current decomposition is given (A-3). Note that, by means of (A-3) the void current of each m-phase is attained from (A-4).

$$i_m = i_{a_m} + i_{r_m} + i_{v_m} = i_{a_m}^{b} + i_{r_m}^{b} + i_{a_m}^{u} + i_{r_m}^{u} + i_{v_m} \tag{A-3}$$

$$i_{v_m} = i_m - \left(i_{a_m}^{b} + i_{r_m}^{b} + i_{a_m}^{u} + i_{r_m}^{u}\right) \tag{A-4}$$

Based on the RMS collective value of the voltages (V_{col}) and P, the balanced active currents can be attained from (A-6). Note that the collective value of a quantity is the Euclidian norm [30]. Analogously, upon the calculation of the RMS collective value of unbiased voltages ($\hat{V}_{col}$) and Q, the balanced reactive currents are given by (A-7). The unbalanced active currents take into account the difference between the phase conductance and the equivalent conductance as seen in (A-8), where V_m and P_m are, respectively, the RMS phase voltage and active power of phase m. Similarly, the unbalanced reactive currents are giving by (A-9).

$$V_{col} = \sqrt{V_a^2 + V_b^2 + V_c^2} \text{ and } \hat{V}_{col} = \sqrt{\hat{V}_a^2 + \hat{V}_b^2 + \hat{V}_c^2} \tag{A-5}$$

$$i_{am}^{b} = \frac{P}{V_{col}^{2}} \cdot v_m, \quad m = a, b, c \tag{A-6}$$

$$i_{rm}^{b} = \frac{Q}{\omega_0 . \hat{V}_{col}^{2}} \cdot \hat{v}_m, \quad m = a, b, c \tag{A-7}$$

$$i_{am}^{u} = \left(\frac{P_m}{V_m^{2}} - \frac{P}{V_{col}^{2}} \right) \cdot v_m, \quad m = a, b, c \tag{A-8}$$

$$i_{rm}^{u} = \left(\frac{Q_m}{\omega_0 . \hat{V}_m^{2}} - \frac{Q}{\omega_0 . \hat{V}_{col}^{2}} \right) \cdot \hat{v}_m, \quad m = a, b, c \tag{A-9}$$

Yet, due to the orthogonality of the CPT's current parcels, the collective current, I_{col}, can be calculated by considering all decomposed terms, as given by (A-10).

$$I_{col}^{2} = \left(I_{a_{col}}^{b}\right)^2 + \left(I_{r_{col}}^{b}\right)^2 + \left(I_{col}^{u}\right)^2 + \left(I_{v_{col}}\right)^2 \tag{A-10}$$

References

[1] B.A. Zavar, E.J.P. Garcia, J.C. Vasquez, J.M. Guerrero, Smart inverters for microgrid applications: a review, MDPI Energies 12 (2019) 1–22.
[2] L.S. Xavier, A.F. Cupertino, H.A. Pereira, V.F. Mendes, Partial Harmonic Current Compensation for Multifunctional Photovoltaic Inverters, IEEE Trans. Power Electron. 34 (2019) 11868–11879.
[3] H.K.M. Paredes, J.P. Bonaldo, J.A. Pomilio, Centralized Control Center Implementation for Synergistic Operation of Distributed Multifunctional Single-Phase Grid-Tie Inverters in a Microgrid, IEEE Trans. Ind. Electron. 65 (2018) 8018–8029.
[4] P. Donolo, et al., Voltage unbalance and harmonic distortion effects on induction motor power, torque and vibrations, Electr. Power Syst. Res. 140 (2016) 866–873.
[5] P.A. Karafotis, V.A. Evangelopoulos, P.S. Georgilakis, Evaluation of harmonic contribution to unbalance in power systems under non-stationary conditions using wavelet packet transform, Electr. Power Syst. Res. 178 (2020) 106026.
[6] H.M.A. Antunes, et al., A new multifunctional converter based on a series compensator applied to AC microgrids, Int. J. Elec. Power Energy Syst. 108 (2018) 160–170.
[7] G. Sun, et al., Multi-functional grid-connected inverter with enhanced disturbance rejection capability, J. Eng. (2019) 3587–3591.
[8] S.Y.M. Mousavi, A. Jalilian, M. Savaghebi, J.M. Guerrero, Power quality enhancement and power management of a multifunctional interfacing inverter for PV and battery energy storage system, Int. Trans. Electr. Energy Syst. 28 (2018) 1 15.
[9] A. Hoke, et al., Setting the smart solar standard: collaborations between hawaiian electric and the national renewable energy laboratory, IEEE Power Energy Mag. 16 (2019) 18–29.
[10] J.M. Guerrero, M. Chandokar, T. Lee, P.C. Loh, Advanced control architectures for intelligent microgrids—Part I: decentralized and hierarchical control, IEEE Trans. Ind. Electron. 60 (2012) 1254–1262.
[11] Y. Han, et al., Review of active and reactive power sharing strategies in hierarchical controlled microgrids, IEEE Trans. Power Electron. 32 (2017) 2427–2451.
[12] Z. Cheng, J. Duan, M. Chow, To centralize or to distribute: that is the question: a comparison of advanced microgrid management systems, IEEE Ind. Electron. Mag. 6 (2018) 24.
[13] Y. Han, K. Zhang, E.A.A. Coelho, J.M. Guerrero, MAS-based distributed coordinated control and optimization in microgrid and microgrid clusters: a comprehensive overview, IEEE Trans. Power Electron. (2018) 6488–6508.
[14] S.Y.M. Mousavi, A. Jalilian, M. Savaghebi, J.M. Guerrero, Coordinated control of multifunctional inverters for voltage supportand harmonic compensation in a grid-connected microgrid, Electr. Power. Syst. Res. (2018) 254–264.
[15] G.G. Talapu, H.M. Suryawanshi, A modified control scheme for power management in an AC microgrid with integration of multiple nanogrids, MDPI Electron. 8 (2019) 1–14.
[16] G. Cavraro, T. Caldognetto, R. Carli, P. Tenti, A master/slave approach to power flow and overvoltage control in low-voltage microgrids, MDPI Energies 12 (2019) 2760.
[17] T.D.C. Busarello, A. Mortezaei, A. Peres, M.G. Simoes, Application of the conservative power theory current decomposition in a load power-sharing strategy among distributed energy resources, IEEE Trans. Ind. Appl. (2018) 3771–3781.
[18] H. Han, et al., Review of power sharing control strategies for islanding operation of AC microgrids, IEEE Trans. Smart Grid 7 (2016) 200–2015.
[19] X. Hou, Y. Sun, W. Yuan, H. Han, C. Zhong, J.M. Guerrero, Conventional P-ω/Q-V droop control in highly resistive line of low-voltage converter-based AC microgrid, MDPI Energies 9 (2016) 1–19.
[20] G. Jin, L. Li, G. Li, Z. Wang, Accurate proportional load sharing among paralleled inverters based on improved P-V droop coefficient, Electr. Power Syst. Res. 143 (2017) 312–320.
[21] S.Y.M. Mousavi, A. Jalilian, M. Savaghebi, J.M. Guerrero, Autonomous control of current and voltage controlled DG interface inverters for reactive power sharing and harmonics compensation in islanded microgrids, IEEE Trans. Power Electron. 33 (2018) 9375–9386.
[22] D.V. Bozalakov, J. Laveyne, J. Desmet, L. Vandevelde, Overvoltage and voltage unbalance mitigation in areas with high penetration of renewable energy resources by using the modified three-phase damping control strategy, Electr. Power Syst. Res. 168 (2019) 283–294.
[23] M. Savaghebi, A. Jalilian, J.C. Vasquez, J.M. Guerrero, Autonomous voltage unbalance compensation in an islanded droop-controlled microgrid, IEEE Trans. Ind. Electron. 60 (2013) 1390–1402.
[24] J. Liu, Y. Miura, T. Ise, Cost-function-based microgrid decentralized control of unbalance and harmonics for simultaneous bus voltage compensation and current sharing, IEEE Trans. Power Electron. 34 (2019) 7373–7410.
[25] E. Espina, et al., Cooperative regulation of imbalances in three-phase four-wire microgrids using single-phase droop control and secondary control algorithms, IEEE Trans. Power Electron. (2019) 1–15.
[26] X. Wu, et al., A two-layer distributed cooperative control method for islanded networked microgrid systems, IEEE Trans. Smart Grid (2019) 1–15.
[27] G. Dehnavi, H.L. Ginn, Distributed load sharing among converters in an autonomous microgrid including PV and wind power units, IEEE Trans. Smart Grid 10 (2019) 4289–4298.
[28] R. Ghanizdeh, G.B. Gharehpetian, Voltage quality and load sharing improvement in islanded microgrids using distributed hierarchical control, IET Ren. Power Gen. 13 (2019) 2888–2898.
[29] Brandao, et al., Coordinated control of distributed three-and single-phase inverters connected to three-phase three-wire microgrids, IEEE J. Emerg. Sel. Top. Power Electron. (2019) 1–16.
[30] P. Tenti, H.K.M. Paredes, P. Mattavelli, Conservative power theory: a framework to approach control and accountability issues in smart microgrids, IEEE Trans. Power Electron. 26 (2011) 664–673.
[31] C. Burgos-Mellado, R. Cardenas, D. Saez, A. Costabeber, M. Summer, A Control algorithm based on the conservative power theory for cooperative sharing of imbalances in four-wire systems, IEEE Trans. Power Electron. 34 (2019) 5325–5339.
[32] A.M.S. Alonso, D.I. Brandao, T. Caldognetto, F.P. Marafao, P. Mattavelli, A selective harmonic compensation and power control approach exploiting distributed electronic converters in microgrids, Int. J. Electr. Power Energy Syst. (2019) 1–15.
[33] A. Mortezaei, M.G. Simoes, M. Savaghebi, J.M. Guerrero, A. Al-Durra, Cooperative control of multi-master–slave islanded microgrid with power quality enhancement based on conservative power theory, IEEE Trans. Smart Grid 9 (2018) 2964–2975.
[34] CK Strunz, et al., Benchmark Systems for Network Integration of Renewable and Distributed Energy Resources - CIGRE WG C6.04 / Task Force C6.04.02 Technical Brochure, Electra 273 (2014) 85–89.
[35] D.I. Brandao, P. Tenti, T. Caldognetto, S. Buso, Control of utility interfaces in low-voltage microgrids, Braz. J. Power Electron. (SOBRAEP) 20 (2015) 373–382.
[36] H. Amaris, et al., Optimal scheduling tools for day-ahead operation and intraday adjustment - Part I: specification and implementation of reference distribution grids and microgrids, IDEAL Grid Project Rep. (2015) 1–76.
[37] IEEE Standard for Interconnection and Interoperability of Distributed Energy Resources with Associated Electric Power Systems Interfaces. IEEE Standard 1547; 2018.
[38] SunSpec Technology Overview. SunSpec Alliance - Technical Note 12040, 2015;1–8.
[39] B. Gharesifar, T. Basar, A.D.D. Gargia, Price-based coordinated aggregation of networked distributed energy resources, IEEE Trans. Aut. Control 61 (2016) 2936–2946.
[40] L.S. Xavier, et al., Adaptive current control strategy for harmonic compensation in single-phase solar inverters, Electr. Power Syst. Res. 142 (2017) 84–95.
[41] D.I. Brandao, et al., Optimized compensation of unwanted current terms by AC power converters under generic voltage conditions, IEEE Trans. Ind. Electron. 63 (2016) 7743–7753.
[42] J. Rocabert, A. Luna, F. Blaabjerg, P. Rodriguez, Control of power converters in AC microgrids, IEEE Trans. Power Electron. 27 (2012) 4734–4749.
[43] P. Mattavelli, F.P. Marafao, Repetitive-based control for selective harmonic compensation in active power filters, IEEE Trans. Ind. Electron. 51 (2004) 1018–1024.
[44] D.I. Brandao, H.K.M. Paredes, A. Costabeber, F.P. Marafao, Flexible active compensation based on load conformity factors applied to non-sinusoidal and asymmetrical voltage conditions, IET Power Electron. 9 (2015) 356–364.
[45] E. Tedeschi, P. Tenti, P. Mattavelli, D. Trombetti, Cooperative control of electronic power processors in micro-grids, Proc. Braz. Power Electron. Conf. (2009) 1–8.
[46] Doğan Çelik, et al., Virtual Park-based control strategy for grid-connected inverter interfaced renewable energy sources, IET Renewable Power Generation 13 (15) (2019) 2840–2852.